The outflow of Asian biomass burning carbonaceous aerosol into the UTLS in spring:

Radiative effects seen in a global model

Prashant Chavan[1,2], Suvarna Fadnavis[1*], Tanusri Chakroborty[1], Christopher E. Sioris[3], Sabine Griessbach[4], Rolf Müller[5]

[1]Indian Institute of Tropical Meteorology, Center for climate change, MoES, India

[2]Savitribai Phule Pune University, Pune, India,

[3]Air Quality Research Division, Environment and Climate Change, Toronto, Canada

[4]Forschungszentrum Jülich GmbH, Jülich Supercomputing Center, Jülich, Germany,

[5]Forschungszentrum Jülich GmbH, IEK7, Jülich, Germany

Corresponding author email: suvarna@tropmet.res.in

Abstract

Biomass burning (BB) over Asia is a strong source of carbonaceous aerosols during spring. From ECHAM6-HAMMOZ model simulations and satellite observations, we show that there is an outflow of Asian BB carbonaceous aerosols into the Upper Troposphere and Lower Stratosphere (UTLS) (black carbon: 0.1 to 6 ng m^{-3} and organic carbon: 0.2 to 10 ng m^{-3}) during the spring season. The model simulations show that the greatest transport of BB carbonaceous aerosols into the UTLS occurs from the Indochina and East Asia region by deep convection over the Malay peninsula and Indonesia. The increase in BB carbonaceous aerosols enhances atmospheric heating by 0.001 to 0.02 K day^{-1} in the UTLS. The aerosol-induced heating and circulation changes increase the water vapour mixing ratios in the upper troposphere (by 20-80 ppmv) and in the lowermost stratosphere (by 0.02-0.3 ppmv) over the tropics. Once in the lower stratosphere, water vapour is further transported to the South Pole by the lowermost branch of the Brewer-Dobson circulation. These aerosols enhance the in-atmosphere radiative forcing (0.68±0.25 W m^{-2} to 5.30±0.37 W m^{-2}), exacerbating atmospheric warming but produce a cooling effect on climate (TOA: -2.38±0.12 W m^{-2} to -7.08±0.72 W m^{-2}). The model simulations also show that Asian carbonaceous aerosols are transported to the Arctic in the troposphere. The maximum enhancement in aerosol extinction is seen at 400 hPa (by 0.0093 km^{-1}) and associated heating rates at 300 hPa (by 0.032 K day^{-1}) in the Arctic.

1. Introduction

There is growing concern about increasing aerosol amounts over South and East Asia, not only because of its contribution to air pollution and its harmful health effects (Chen et al., 2017; Thomas et al., 2019), but also because of its impact on the hydrological cycle (Meehl et al., 2008). Biomass burning (BB) accounts for ~60% of the total aerosol optical depth (AOD) globally (Cheng et al., 2009; Streets et al., 2003). It is one of the major sources of large carbonaceous aerosol (Ni et al., 2019). BB is responsible for the major fraction of global mean emissions of black carbon (BC, ~59%) and organic carbon (OC, ~85%) (Bond et al., 2013).

In Asia, China (25%) is the largest contributor to the global BB aerosol emissions, followed by India (18%), Indonesia (13%), and Myanmar (8%) (Streets et al., 2003). Among the sources, forest burning (anthropogenic and natural) contributes 45%, burning of crop residues in the field 35%, and burning grassland and savannah 20% to the total BB aerosols in Asia (Streets et al., 2003). Asia emits a substantial amount of BC (~ 0.45 Tg yr^{-1}) and OC (~3.3 Tg yr^{-1}) from BB (Streets et al., 2003). These are significant fractions of the global BB emissions of BC (~2.8–4.9 Tg yr^{-1}) and OC (~31–36 Tg yr^{-1}), respectively (Andreae, 2019). Recently, Wu et al. (2018) and Singh et al. (2020) reported ~83% of the carbonaceous aerosol mass is emitted from open fires over South and East Asia. Within Asia, BB carbonaceous aerosol emissions from East Asia (BC: 110 Gg, OC: 730 Gg) are larger than over India (BC: 83 Gg, OC: 650 Gg) and the Indochina region (BC: 40 Gg, OC: 310 Gg) (Streets et al., 2003).

Biomass burning over Asia shows a strong seasonal cycle peaking in spring (Streets et al., 2003). Our analysis of MODIS fire counts over Asia also shows a pronounced peak in spring (Fig. 1a). The carbonaceous aerosols emitted from BB also peak in spring over Indochina, South Asia, and East Asia regions (Fig. 1b). These aerosols will affect the regional radiative forcing. The literature shows that aerosols emitted from BB in spring produce a significant negative radiative forcing at the top of the atmosphere (TOA) and at the surface, but in-atmospheric radiative forcing (TOA - surface) is positive over Asia (Wang et al., 2007; Lin et al., 2014; Singh et al., 2020).

Deep convection occurs over the Bay of Bengal, the South China Sea, and Malay Peninsula during the spring and monsoon seasons (Randel et al., 2010; Fadnavis et al., 2013; Murugavel et al., 2012) that may transport Asian boundary layer pollutants to the UTLS. Numerous airborne measurements show evidence of carbonaceous aerosol in the upper troposphere over Asia and adjoining outflow regions during spring and monsoon seasons, e.g., measurements from the Civil Aircraft for Regular Investigation of the Atmosphere Based on an Instrument Container (CARIBIC) campaign in 2004, Stratospheric and upper tropospheric processes for better climate predictions (StratoClim) in 2017, Aerosol Radiative Forcing in East Asia (A-FORCE) in 2009, and Transport and Chemical Evolution over the Pacific (TRACE-P) in 2001 (Nguyen et al., 2008; Pozzoli et al., 2008; Oshima et al., 2012; Weigel et al., 2020; Brunamonti et al., 2018; Hanumanthu et al., 2020). There may be a significant contribution from BB to the observed carbonaceous aerosols in the UTLS, since BB accounts for ~59 - 80 % of the carbonaceous aerosols globally (Bond et al., 2013) and being fine-grained, these aerosols have long atmospheric residence times. Transport of Australian wildfire smoke into the stratosphere (~35km) is seen in satellite observations (Khaykin et al., 2020). The balloon-borne, lidar, and satellite observations showed pyro-

cumulonimbus events that injected smoke from Canadian forest fires into the stratosphere in August 2017 (Peterson et al., 2018; Hooghiem et al., 2020; Lestrelin et al., 2021). The carbonaceous aerosols were transported to the upper troposphere and produced significant heating locally (Fadnavis et al., 2017a). The heating of the upper troposphere induces an amplification of the vertical motion in the troposphere (Fadnavis et al., 2017b; Hooghiem, et al., 2020).

Numerous studies show the transport of boundary layer aerosols from Asia to the lower stratosphere during the monsoon season (Randel et al., 2010; Fadnavis et al., 2013). However, transport of Asian aerosol pollution into the UTLS during the spring season is not reported hitherto when the deep convection occurs over the Malay peninsula (Chang et al., 2005) and Indonesia, and when biomass burning aerosol emissions show a peak (Streets et al., 2003; Fig. 1). In this study, we address these unexplored science questions (1) transport pathways of Asian BB aerosols to the lower stratosphere during the spring season, (2) impacts of Asian BB carbonaceous aerosols on the lower stratosphere. For this purpose, we employ the state-of-the-art ECHAM6-HAMMOZ chemistry-climate model. The model is evaluated against satellite (MODIS) and ground-based remote sensing (AERONET). The paper is organized as follows: satellite data, ground-based data and the experimental set-up are described in section 2. Section 3 comprises a discussion on the distribution of fires and model evaluation; results are discussed in section 4; conclusions are given in section 5.

2. Model simulations and satellite observations

2.1 Model description and experimental set-up

The fully coupled chemistry-climate model ECHAM6.3–HAM2.3 is used in this study. It comprises the general circulation model ECHAM6 coupled to the aerosol sub-module "Hamburg Aerosol Model (HAM)" (Stier et al., 2005). HAM predicts the evolution of sulfate (SU), BC, OC, particulate organic matter (POM), sea salt (SS), and mineral dust (DU) aerosols. The size distribution of the aerosol population is described by seven lognormal modes with prescribed variance in the aerosol module (Stier et al., 2005). The anthropogenic and fire emissions were obtained from the ACCMIP-II (Emissions for Atmospheric Chemistry and Climate Model Intercomparison Project) emission inventories and are interpolated for the period 2000 - 2100 by using Representative Concentration Pathway 4.5 (RCP4.5) (Lamarque et al., 2010; van Vuuren et al., 2011). The biomass burning emissions dataset represent average conditions of the decade (Tegen et al., 2019). It should be noted that inter-annual variability of biomass burning is not considered in our simulations. Injection heights of biomass burning emissions are documented by Val Martin et al. (2010). The majority (75%) of the emissions are evenly distributed within the planetary boundary layer (PBL) with 17% in the first model level above the planetary boundary layer and 8% in the second model level above the planetary boundary layer (Tegen et al., 2019). Biogenic emissions are derived from MEGAN (Guenther 1995). In the model, biogenic OC is directly inserted via emissions. Secondary organic aerosol (SOA) emissions are as described by Dentener et al. (2006).

The model simulations are performed at a T63 spectral resolution corresponding to $1.875° \times 1.875°$ horizontal resolution, while 47 hybrid σ-p levels provide the vertical

129   resolution from the surface up to 0.01 hPa. The model has 12 vertical levels in the UTLS

130   (300 to 50 hPa). The simulations have been carried out at a time step of 20 min. Atmospheric

131   Model Inter-comparison Project (AMIP) monthly varying sea surface temperature (SST) and

132   sea ice cover (SIC) were used as lower boundary conditions. We performed two sets of

133   emission sensitivity experiments; in one set of the simulations, the aerosol emissions from

134   biomass burning were kept on (referred to as BMaeroon simulations) and in another set of the

135   simulations, the aerosol emissions from biomass burning were kept off (referred to as

136   BMaerooff simulations). We adopted an ensemble mean approach (with ten ensemble

137   members) for the above two experiments. Ten spin-up simulations were performed from 1-10

138   January 2012 up to 28 February 2013 to generate stabilized initial fields for the ten ensemble

139   members. Emissions were the same in each of the ten members during the spin-up period. In

140   the BMaerooff simulations (ten ensemble members each), the biomass burning aerosols were

141   switched off since 1 March 2013. The BMaeroon and BMaerooff simulations ended on 31

142   December 2013. To investigate the effects of biomass burning aerosol emissions in spring

143   (i.e., since 1 March 2013), we analyze the difference between BMaeroon and BMaerooff

144   simulations for the spring season in 2013. The uncertainty estimates in simulated radiative

145   forcing, heating rates, aerosol extinction coefficient are obtained from the 10 members of the

146   different initial conditions. The year 2013 was chosen for the analysis as this was a neutral

147   year without a pronounced El Niño or Indian Ocean Dipole oscillation. Such large-scale

148   coupled atmosphere–ocean oscillations substantially affect the transport processes to the

149   UTLS (Fadnavis et al., 2017a, 2019).

150

151

152

153

2.2 MODIS fire counts and aerosol optical depth

In order to study spatio-temporal variations in the biomass burning activity, we analysed the Terra/Aqua combined daily active fire location data (product mcd14dl) from the Moderate Resolution Imaging Spectroradiometer (MODIS) (https://firms.modaps.eosdis.nasa.gov/download/) onboard Terra and Aqua (Earth Observing System). This MODIS collection-6, Level-2 global data are processed by NASA's Land, Atmosphere Near real-time Capability for EOS (LANCE) Fire Information for Resource Management System (FIRMS), using swath products (MOD14/MYD14). The thermal anomaly / active fire represents the centre of a 1 km pixel that is flagged by the MODIS MOD14/MYD14 Fire and Thermal Anomalies algorithm as containing one or more fires within the pixel (Giglio et al., 2003). The fire detection algorithm uses the strong mid-infrared (IR) emissions from the fires (Matson and Dozier 1981) and is based on the brightness temperatures derived from MODIS at the 4 and 11-μm channels. The retrieval algorithm classifies fire pixels in three categories: low confidence (0 – 30 %), nominal confidence (30 – 80 %), and high confidence (>80 %). This confidence limit allows the rejection of false fires (Giglio, 2015). Here, data with high or nominal confidence (≥70 %) are used.

For information on aerosol, we used monthly mean data from MODIS Terra (MOD08 M3 V6.1) at 1°×1° horizontal resolution to study AOD variability over the Asian region during spring 2013. MODIS Terra measures radiance emanating from the surface and the atmosphere and provides images in 36 spectral bands between 0.415 and 14.235 μm, with a spatial resolution varying from 250 m to 1 km (Mhawish et al., 2019). Terra MODIS

178 MOD08_M3 (V6.1) aerosol products (i.e., AOD) are retrieved using the Deep Blue (DB)

179 algorithm. The algorithm calculates the column aerosol loading at 0.55 μm over land and

180 ocean.

181

182 **2.3 Multi-Angle Imaging Spectroradiometer (MISR), Aerosol Robotic NETwork**

183 **(AERONET) and Optical Spectrograph and InfraRed Imaging System (OSIRIS)**

184 **observations**

185

186   The AOD retrievals from the Multi-Angle Imaging Spectroradiometer (MISR) at 550

187 nm wavelength and the Aerosol Robotic NETwork (AERONET) sunphotometer during

188 spring 2013 are also used for comparison with the model simulations. Details of MISR are

189 available   at   https://misr.jpl.nasa.gov/getData/accessData/   and   AERONET   at

190 https://aeronet.gsfc.nasa.gov/. AERONET AOD observations are obtained at different stations

191 in the Indochina region (Myanmar: 16.86°N - 96.15°E, Vientiane: 17.99°N-102.57°E,

192 Siplakorn University: 13.81°N-100.04°E, Ubon-Ratchathani: 15.24°N - 104.87°E), South

193 Asia (Gandhi college: 25.81°N - 85.12°E, Lumbini: 27.49°N-83.28°E, Kathmandu Bode:

194 27.68°N -85.39°E, Dhaka University: 23.72°N - 90.39°E), East Asia (Nghia-Do: 21.04°N -

195 105.80°E, Hong Kong Polytechnic University: 22.30°N - 114.18°E).

196

197   We compared simulated aerosol extinction coefficient vertical profiles with

198 observations from Optical Spectrograph and InfraRed Imaging System (OSIRIS) on-board

199 the Odin satellite (Bourassa et al., 2012). We used version 7.0 vertical profiles of aerosol

200 extinction at 750 nm for March-May 2013 (https://research-groups.usask.ca/osiris/data-

201 products.php#Download). The limb scatter measurements from OSIRIS show good

202 agreement with Stratospheric Aerosol and Gas Experiment (SAGE) II and Scanning Imaging

Absorption spectrometer for Atmospheric Chartography (Rieger et al., 2018). To understand convective activity in spring 2013, we also analyzed Outgoing Longwave Radiation (OLR) data for March - May 2013 from the National Center for Environmental Prediction (NCEP) re-analysis-2 (https://psl.noaa.gov/data/gridded/data.ncep.reanalysis2.pressure.html).

3. Distribution of fires and model evaluation

3.1 Seasonal distribution of fires over Asia

In this section, we discuss the seasonal variability of fire activity in Asia. The fire counts peak over Asia (10°S - 50°N, 60°E - 130°E) in the spring season. Figure 1a-b shows that fires are clustered over three sub-regions (1) Indochina region (91°E - 107°E, 10°N - 27°N) (numbers of fire counts: 80694), (2) East Asia (108°E - 123°E, 22°N - 32°N), (numbers of fire counts: 4770), (3) South Asia (65°E - 90°E, 8°N - 32°N) (numbers of fire counts: 14223) (Fig. 1b). Fire counts over the three sub-regions peak in spring although the month varies, e.g., fire counts over East Asia show a peak in March, Indochina region in March-April, and South Asia in May (Fig. 1a). The fire counts over South Asia show a secondary peak in October. In agreement with our results, Bhardwaj et al. (2016) also reported high fire activity in spring and the lowest fire activity during the monsoon (June–September) in the 2003-2013 time frame. Streets et al. (2003) reported that higher fire counts during the spring season over South Asia and East Asia are attributed to enhanced crop burning activity. Over the Indochina region, high fire counts are associated with forest fires along with crop burning. Intense biomass burning activity over Asia during the spring season is also reported by Zhang et al. (2020). Hence, we provide further analysis in spring.

3.2. Model evaluation

We compare simulated AOD (averaged for spring from BMaeroon simulations) with MODIS, MISR, and AERONET. Figure 2 (a-c) shows large AOD over the regions: Indochina (MODIS: ~0.4 to 0.8, MISR: 0.27 to 0.6; model: 0.27 to 0.5), East Asia (MODIS: 0.5 to 1.3, MISR: 0.27 to 1, model: 0.5 to 1.4), and the Indo-Gangetic plain in south Asia (23°N -30°N, 75°E - 85°E) (MODIS: 0.24 to 0.8, MISR: 0.24 to 0.5, model: 0.3 to 0.6). The MISR AOD is comparatively less than MODIS AOD over all three study regions (Fig. 2a-b). There are differences in the spatial distribution of AOD among MODIS, MISR and the model. Over East Asia, the model overestimates AOD relative to MISR (by 0.24) and MODIS (by 0.1). Over Indochina, the model shows an underestimation compared to MISR (by 0.1) and MODIS (by 0.2). The simulated AOD is over-estimated over the Indo-Gangetic plain in comparison with MISR (by 0.08) and underestimated compared to MODIS (0.2). The simulated AOD is underestimated south of 13°N compared to MISR and MODIS (MODIS: 0.4 to 0.7, MISR:0.4 to 0.6, model: 0.21 to 0.3) and overestimated over central India (lat: 20° - 28°N lon: 75°E - 88°E) compared to MODIS and MISR (MODIS:0.16 to 0.4, MISR:0.21 to 0.3, model: 0.3 to 0.5). These issues may be due to a higher amount of dust emission in the model over West Asia that is transported to India. In the past, a number of papers reported that transport of dust occurs from west Asia to the Indo-Gangetic plain and the Tibetan Plateau region during spring (Lau and Kim 2006; Fadnavis et al., 2017b, Fadnavis et al., 2021a). Simulated AOD is also overestimated over the Tibetan Plateau and East Asian region (MODIS: 0.21 to 1.0, MISR: 0.16 to 0.6, model: 0.27 to 1.2). The distribution of dust AOD also shows high amounts over these regions (See Fig. S1). This indicates that higher amounts of dust over the Tibetan Plateau and the East Asia region cause overestimation of AOD there. Tegen et al. (2019) also reported that in ECHAM6–HAMMOZ simulations the AOD is

overestimated over East Asia in comparison with MISR. The model simulations underestimate the AOD over the Himalayas in comparison with MODIS (MODIS: 0.24 to 0.3, MISR: 0.1 to 0.21, model: 0.1 to 0.3). It should be noted that dust emission/parameterization is the same in both BMaeroon and BMaerooff simulations.

Further, we compare simulated AOD with ground-based measurements at ten AERONET stations during spring 2013 (Figure 2d). Model results were sampled at each station at the same time. Comparison with AERONET observations also shows that the model underestimates AOD over all the stations. The simulated AOD (0.54) shows the highest underestimation at Nghia Do (21.04°N - 105.80°E) in East Asia and the lowest underestimation at Gandhi college (25.81°N - 85.12°E) in the Indo-Gangetic plain, where the simulated 550 nm AOD is 0.57.

The differences in the magnitude of AOD between model, satellite remote sensing (MISR, MODIS), and ground-based AERONET observations may be caused by various factors; e.g., satellite remote sensing of AOD exhibits biases over certain surface types. The differences between MISR and MODIS may be due to differences in their calibration, algorithm assumptions, or the aerosol models in the lookup tables used in the retrieval algorithms (Addou et al., 2005; Choi et al., 2019). There are uncertainties in the model emission inventories (Fadnavis et al., 2013, 2017, 2019).

The vertical distribution of simulated aerosol extinction coefficient profiles (BMaeroon) averaged over the BB burning region (10ºN - 30ºN) are compared with OSIRIS observations in spring 2013 (Fig. 2e-f). Our model could simulate vertical variations similar to those observed by OSIRIS. A plume rising from 90ºE - 120ºE extends to 16 km is also

278 evident in the OSIRIS data although the model underestimates the aerosol extinction

279 coefficient by 0.0002 - 0.0003 km^{-1}. The sign of the difference is consistent with the slightly

280 shorter wavelength of the OSIRIS extinction measurements. This underestimation may also

281 be due to uncertainties in the model due to emission inventory and transport processes in the

282 model. It should be noted that there may be biases in OSIRIS measurements due to

283 assumptions made on the aerosol size distribution and chemical composition (Bourassa et al.,

284 2012).

285

286 **4. Results**

287 **4.1 Impact of biomass burning on Aerosol Optical Depth (AOD)**

288

289 Figure 3 (a) shows the distribution of anomalies in simulated AOD (BMaeroon-

290 BMaerooff). It shows enhanced AOD anomalies over the Indo-Gangetic plain (~0.22 to 0.8),

291 the Tibetan Plateau and the north eastern parts of East Asia (~0.3 to 1.2). The distribution of

292 anomalies in dust AOD shows high amounts over these regions. It indicates that dust

293 enhancement over the Indo-Gangetic plain (~0.22 to 0.8), the Tibetan Plateau and the

294 northeastern parts of East Asia (0.8 to 1) (Fig. 3b) causes enhancement in AOD there. The

295 simulated dust anomalies and circulation patterns also show transport of enhanced dust from

296 West Asia to North India and the Indo-Gangetic plain region in the lower troposphere (Fig. 3b

297 and Fig. S2a). Dust is also transported from Tibetan Plateau-East Asia region to North India

298 in the mid/upper troposphere (Fig. S2b). The enhanced dust transport from west Asia and

299 Tibetan Plateau-East Asia region to South Asia is induced by atmospheric heating generated

300 by biomass burning carbonaceous aerosols (discussed in section 4.4). This atmospheric

301 heating leads to enhanced dust emission over the respective desert regions. Dust being

302 absorptive in nature contributes to a further increase of the atmospheric heating. The heating

12

303 led to a formation of a low pressure zone over East India in the lower troposphere (900 hPa)

304 (Fig. 3b) and the Bay of Bengal and Myanmar in the mid-troposphere (500 hPa) (Fig. S2b

305 and Fig. 7b). These circulation changes further enhanced the dust transport from west Asia

306 and the Tibetan Plateau-East Asia region to South Asia.

307

308   Figure 3c shows the spatial distribution of the AOD for carbonaceous aerosols

309 (BC+OC). The changes in concentration of total column carbonaceous aerosols are shown in

310 Fig. S3a. Figures 3c and S3a show increases in aerosols over Indochina (AOD: +0.04-0.07,

311 concentration: +40-80%), Indo-Gangetic plain (AOD: +0.014-0.03, concentration: +10-50%)

312 and East Asia (AOD: +0.018-0.04, concentration: +20-60%). It is evident that anomalies of

313 carbonaceous aerosols AOD over the Indo-Gangetic plain and East Asia are comparatively

314 lower than over the Indochina region. In agreement with our results, Wang et al. (2015) also

315 reported an abundant mixture of BC and OC particles due to BB over the Indochina region in

316 spring 2014. Our model simulations show that the contribution of BB-emitted OC to AOD

317 (Indochina 16 to 35 %; East Asia: 4 to 12 %; South Asia: 0.8 to 4 %) is higher than that of

318 BB-emitted BC (Indochina: 1.8 to 6 %; East Asia: 0.8 to 1.4 %; South Asia: 0.2 to 0.8 %)

319 (Fig. S3b-c). Figure 3c also shows high amounts of carbonaceous aerosols over the western

320 Pacific, which may be due to transport from the Indochina region by westerly winds

321 (discussed later in subsection 4.3).

322

323 **4.2. Impact of BB carbonaceous aerosol on radiative forcing**

324

325   The carbonaceous aerosols emitted from biomass burning may significantly change

326 radiative forcing by absorption and attenuation of solar and terrestrial radiation (Schill et al.,

327 2020). The anomalies (averaged for spring) in net radiative forcing show negative radiative

328   forcing at the surface and top of the atmosphere (TOA) over South Asia (surface: -5.08±0.44

329   W m^{-2}; TOA: -4.39±0.26 W m^{-2}), Indochina region (surface:-7.68±0.45 W m^{-2}; TOA: -

330   2.38±0.12 W m^{-2}) and East Asia (surface:-10.81±0.63 W m^{-2}; TOA: -7.08±0.74 W m^{-2}) (Fig.

331   4). The estimates of in-atmosphere radiative forcing show positive anomalies over south Asia

332   (0.68±0.25 W m^{-2}), Indochina region (5.30±0.37 W m^{-2}), and East Asia (3.73±0.20 W m^{-2}),

333   indicating an atmospheric warming. In agreement with our study, a number of studies showed

334   a negative radiative impact at the TOA and surface, but positive in-atmosphere radiative

335   forcing due to BC and OC aerosols over the Indochina region. For example, Lin et al. (2014)

336   reported a radiative forcing of -4.74 W m^{-2} at the TOA, -26.85 W m^{-2} at the surface, thus

337   +22.11 W m^{-2} in-atmosphere. Wang et al. (2007) estimated a radiative forcing of -1.4 to -1.9

338   W m^{-2} at the TOA and -4.5 to -6 W m^{-2} at the surface, yielding +2.6 W m^{-2} in-atmosphere

339   during March 2001. Singh et al. (2020) also reported a radiative forcing at the TOA of -1.91

340   W m^{-2} and -42.76 W m^{-2} at the surface and 40.85 W m^{-2} in-atmosphere over Myanmar.

341

342   **4.3. Transport of biomass burning aerosol into the upper troposphere and lower**

343   **stratosphere**

344

345   The stepwise evolution of the Asian summer monsoon begins in spring and contributes a

346   significant amount of rainfall to the total annual precipitation over China (25–40%) and over

347   South Asia (~11-20%) due to deep convection over the Bay of Bengal, Tibetan Plateau and

348   South China Sea (Guhathakurta and Rajeevan, 2008; Li et al., 2016). The distribution of

349   outgoing long-wave radiation (OLR) from NCEP reanalysis data during the spring season

350   confirms that deep convection occurs over the maritime continent that extends to the South

351   China Sea, Bay of Bengal, Malay Peninsula and Indonesia (Fig. 5a). Our model simulation

352   shows a distribution of OLR similar to the observations, although OLR is overestimated in

the model (Fig. 5b). Figure 5(c)-(d) shows the combined distribution of Cloud Droplet Number Concentration (CDNC), Ice Crystal Number Concentration (ICNC), and vectors of the resolved circulation, which exhibit a strong upwelling in equatorial Asia (10°N - 20°N, 85°E - 140°E, Fig. 5c-d). This upwelling associated with deep convection may transport pollutants from the boundary layer into the UTLS.

We analyzed the vertical distribution of simulated anomalies (BMaeroon - BMaerooff) of BB carbonaceous aerosols obtained over the high fire emission regions, i.e., Indochina, South Asia, and East Asia in spring 2013 (Fig. 1b). The simulated distribution of BC aerosols (Fig. 6 a-b) and OC aerosols (Fig. 6c-d) over the Indochina region indicates an aerosol plume extending to the lowermost stratosphere. The ascent resolved in the wind vectors together with the distribution of cloud droplets and cloud ice indicate that the transport of these aerosols from the surface to the lowermost stratosphere occurs due to deep convection over the Malay peninsula and Indonesia (Fig. 5a-b). There is an enhancement of BC aerosol concentration by $0.1 - 2$ ng m^{-3} (Fig. 6 a-b) and for OC by $0.2 - 5$ ng m^{-3} (Fig. 6 c-d) in the UTLS (300 - 90 hPa) over the Indochina region.

In the troposphere, biomass-burning carbonaceous aerosols are transported to the Arctic (Fig. 6a and Fig. 6c). Some previous studies also show aerosol transport from South Asia and East Asia to the Arctic (Shindell et al., 2008; Fisher et al., 2011). The carbonaceous aerosols are also transported towards the Western Pacific (Fig. 6 b-d and 6 f-h). In the Pacific (140ºE - 170ºW), these aerosols are lifted to the UTLS. Transport of the aerosols from the Indochina region to the Western Pacific has also been reported in the past (Dong and Fu, 2015).

378   Further, we show the distribution of BB carbonaceous aerosol over East Asia in

379   Figure 6 e-h. It shows that the plume of BC and OC aerosol crosses the tropopause (BC: 0.2–

380   6 ng m^{-3} and OC: 0.2 to 10 ng m^{-3}). Figures 6e and 6g also show that the aerosol plume from

381   the equatorial region is lifted to the UTLS associated with the Indonesian region (130°E -

382   170°E). Similar to the Indochina region, BC and OC aerosols also show poleward transport

383   to the Arctic and horizontal transport towards the Western Pacific (Figures 6f and 6h). These

384   aerosols are vertically transported in the western Pacific region (130°E - 170°E). The

385   distribution of anomalies of BC and OC near the tropopause (at 100 hPa) shows outflow of

386   Asian carbonaceous aerosols in the UTLS over equatorial Asia and Western Pacific (5°S-

387   20°N, 70°E - 180°E) (Fig. S4).

388

389   BB in South Asia occurs in central India (70°E - 90°E, 8°N -24°N) in spring (Fig. 1 b

390   and Singh et al., 2017). BC and OC emissions over South Asia during the spring season are

391   reported in many studies (Talukdar et al., 2015; Guha et al., 2015). The vertical distribution

392   of anomalies of BC and OC over south Asia shows that positive anomalies of BC and OC

393   aerosols extend from the surface to the upper troposphere (300 hPa) (Fig. S5). CALIPSO

394   derived aerosol profiles in spring 2013 also show plumes reaching up to approximately 7 km

395   (400 hPa) (Singh et al., 2020). Unlike the Indochina region, BB carbonaceous aerosols over

396   Indo-Gangetic plain do not reach the lowermost stratosphere during the spring season.

397   Hence, hereafter we focus our discussion on the transport of BB carbonaceous aerosols and

398   their impacts on the UTLS for Indochina and East Asia.

399

400   Further, we analyze the aerosol enhancement over the Arctic (65°N - 85°N) due to the

401   transport of Asian biomass burning BC and OC aerosols. The vertical distribution of

402   anomalies of aerosol extinction shows an enhancement of 0-0.0093 km^{-1} in the Arctic (1000 -

16

403   100hPa) with a peak at 400 hPa (Fig. 7a). Shindell et al. (2008) also showed seasonally

404   varying transport of South Asian aerosols to the Arctic that maximizes in the spring season.

405

406   **4.4 Impact of BB carbonaceous aerosol on heating rates**

407

408   Carbonaceous aerosols in the atmosphere produce significant heating leading to

409   atmospheric warming (Fadnavis et al., 2017b). We obtained anomalies in heating rates

410   (shortwave + longwave) due to carbonaceous aerosols (BMaeroon - BMaerooff). Figure 7b

411   shows the spatial distribution of anomalies in tropospheric heating rates (averaged from

412   surface to tropopause). It shows that carbonaceous aerosols have induced significant

413   tropospheric heating over the location of dense fires; Indo-China/East Asia (0.02 to 0.12

414   K.day^{-1}). Significant heating is seen namely over the Mongolian desert (0.08 - 0.12 K.day^{-1}).

415   The desert region of west Asia (Pakistan, Afghanistan, Turkistan, Kazakhstan) also shows

416   slight heating (0.02 - 0.04 K.day^{-1}). The heating over the desert regions is associated with

417   enhanced emission of dust, a positive feedback to atmospheric heating induced by the

418   carbonaceous aerosols (section 4.1). Heating is higher over the Mongolian desert than over

419   west Asia due to the vicinity of Mongolia to the location of dense fires.

420

421   Further we show the vertical distribution of heating rates over the Indochina region

422   and East Asia in Figures 8a-d. It shows that enhanced BB carbonaceous aerosols have

423   induced enhanced heating of the atmospheric column along the pathway through which they

424   are transported (Fig. 6a-h). The carbonaceous aerosol emissions over the Indochina region

425   and East Asia produced anomalous heating of ~0.1 to 0.04 K day^{-1} in the lower troposphere

426   (1000 hPa to 400 hPa) and ~0.008 to 0.001 K day^{-1} near the tropopause (200 hPa to 80 hPa).

427   Figure 6 a, c, e, g shows that descending winds transport BC and OC aerosols from above the

428 tropopause downward and southward to 20°S. The positive anomalies in heating rates of

429 ~0.001 to 0.004 K day^{-1} in the upper troposphere at ~200 hPa near 20ºS may be due to

430 heating by these aerosols. There may be dynamic changes in response to BB carbonaceous

431 aerosol emission. The transported Asian carbonaceous aerosols and associated dynamical

432 changes in the Arctic enhanced heating rates by 0 - 0.032 K day^{-1} between 1000 - 100 hPa

433 (Fig. 7a). Also, transport of carbonaceous aerosol to the western Pacific (Fig. 6 b, d, f, h) by

434 the westerly winds has increased heating by 0.008 to 0.04 K day^{-1} and peaks at 250 hPa (0.04

435 K day^{-1}) over the Central Pacific (170°W - 110°W).

436

437   Figure 8 (a-d) shows positive anomalies in heating rates at the tropopause. Heating in

438 the upper troposphere enhances the vertical motion that may enhance the transport into the

439 lower stratosphere (Gettelman et al., 2004). Carbonaceous aerosols cross the tropopause (0.1

440 to 5 ng m^{-3}) and enter the lowermost stratosphere (18ºN - 24ºN) (Figs. 6 a-h). The cross

441 tropopause transport is reinforced by enhanced vertical motion (Fig. S6a-b) produced by the

442 heating generated by the carbonaceous aerosols.

443

444 **4.5 Impact of BB carbonaceous aerosol on water vapor**

445

446   The heating produced by the biomass burning carbonaceous aerosols may affect the

447 distribution of water vapor in the troposphere and stratosphere. Figure 9a-b shows anomalies

448 in water vapor (BMaeroon - BMaerooff) over Indochina and East Asia. An interesting feature

449 seen in Fig. 9a-b is the enhanced transport of water vapor (an anomaly of 0.02 - 0.5 ppmv) to

450 the South Pole through the lower stratosphere from Indochina (91°E - 107°E, 10°N - 27ºN)

451 and East Asia (108°E - 123°E, 20°N - 35°N). The tropospheric heating might have caused

452 elevated water vapor injection into the lower-stratosphere. The water vapour in the lower

453 stratosphere is further transported to the South Pole by the lower branch of the Brewer-

454 Dobson circulation. The water vapour reaches the Antarctic within a month indicating fast

455 transport.

456

457   The model simulations show noticeable enhancement of water vapor (0.4 to 1.6

458 ppmv) in the northern tropics near the tropopause (150 hPa) and by 0.2 - 0.7 ppmv in the

459 Arctic lower stratosphere (150 hPa) (Fig. 9c). In the tropical lower stratosphere, it is

460 increased by 0.02 - 0.3 ppmv (Fig. 9d). Water vapor, being a greenhouse gas, amplifies global

461 warming leading to positive feedback (e.g., Riese et al., 2012; Sherwood et al., 2018,

462 Fadnavis et al., 2021b). The strong negative anomalies of OLR (Fig. S6c) induced by

463 carbonaceous aerosols also indicate the positive feedback. Fadnavis et al. (2013) also

464 reported an increase in water vapor in the UTLS in response to the enhancement of aerosols.

465 Stratospheric water vapor plays a significant role in climate change (e.g., Oman et al., 2008;

466 Wang et al., 2020; Xie et al., 2020).

467

468 **5. Conclusions**

469

470   A ten-member ensemble of ECHAM6.3–HAM2.3 simulations for the spring season

471 2013, a neutral year, is analyzed to study the transport of carbonaceous aerosol injected by

472 Asian biomass burning into the UTLS and its associated impacts on radiative forcing, heating

473 rates, and water vapor. To validate the model simulations, we compare simulations with

474 observations from (1) MODIS, (2) MISR, (3) AERONET, (4) OSIRIS during spring 2013.

475 The observational analysis shows reasonable agreement with the model simulations.

476

477   The BB emission increases the aerosol burden (AOD) over the Indochina region by

478   0.14 to 0.22 (carbonaceous aerosol concentration increase of +40-80%), India by 0.22 to 0.38

479   (concentration of carbonaceous aerosol: +10-50%), and East Asia by 0.18 to 0.26

480   (concentration of carbonaceous aerosol: +20-60%).Our analysis shows that deep convection,

481   which occurs over the Malay peninsula and Indonesia, transports carbonaceous aerosols

482   from the boundary layer of the Indochina and East Asia region into the lowermost

483   stratosphere (BC: 0.1 to 6 ng m^{-3} for BC, OC: 0.2 to 10 ng m^{-3}). In the UTLS, outflow occurs

484   over equatorial Asia and the Western Pacific (10°S - 20°N, 70°E - 180°E). Carbonaceous

485   aerosols originating from Asian biomass burning are also transported to the Arctic. The

486   maximum enhancement in aerosol extinction (by 0.0093 km^{-1}) is seen at 400 hPa over the

487   Arctic.

488

489   The enhanced carbonaceous BC and OC aerosol emitted from BB produces a negative

490   net radiative forcing at the surface (India: -5.08±0.44 W m^{-2}, Indochina: -7.68±0.45 W m^{-2},

491   and East Asia: -10.81±0.63 W m^{-2}), at the TOA (India: -4.39±0.26 W m^{-2} , Indochina: -

492   2.38±0.12 W m^{-2}, and East Asia: -7.08±0.74 W m^{-2}) and positive net radiative forcing in the

493   atmosphere (India: 0.68±0.25 W m^{-2}, Indochina: 5.30±0.37 W m^{-2}, and East Asia: 3.73±0.20

494   W m^{-2}) indicating atmospheric warming, but a cooling of the climate at the surface.

495

496   The changes in BB carbonaceous aerosol induce a warming in the troposphere (0.008

497   – 0.1 K day^{-1}) and in the UTLS (~0.001 to 0.008 K day^{-1}) over Asia. The aerosols transported

498   to the Arctic enhance heating by 0 - 0.032 K day^{-1}, peaking at 300 hPa. The outflow of the

499   aerosols in the UTLS over the western Pacific by the westerly winds has increased heating by

500   0.008 to 0.04 K day^{-1}. The atmospheric heating induced by Asian BB carbonaceous aerosols

501   led to the transport of water vapor into the lower stratosphere (0.02 - 0.3 ppmv) over the

502 tropics. In the lower stratosphere, water vapour is transported to the South Pole by the lower

503 branch of the Brewer-Dobson circulation. Water vapor, being a greenhouse gas, amplifies

504 atmospheric heating, leading to positive feedback (e.g., Riese et al., 2012; Sherwood et al.,

505 2018). Our model simulations also show a positive feedback of dust aerosol on atmospheric

506 heating induced by the enhancement of carbonaceous aerosols.

507

508 Furthermore, our analysis shows that Asian biomass burning carbonaceous aerosols

509 lead to moistening of the troposphere in the northern hemisphere and lowermost stratosphere

510 in the northern tropics and southern hemisphere. An increase in stratospheric water vapour is

511 important as it has an impact on stratospheric temperatures and thus indirectly on

512 stratospheric dynamics (Maycock et al., 2013). The moistening of the stratosphere produces a

513 positive feedback on the climate (Banerjee et al., 2019; Dessler et al., 2013).

514

519

520   **Data availability:** The MODIS fire count data were downloaded from

521   https://firms.modaps.eosdis.nasa.gov/download. The AOD data from MODIS Terra can be

522   downloaded from https://ladsweb.modaps.eosdis.nasa.gov/archive/allData/61/MODATML2/

523   The AOD data from MISR were obtained from

524   https://misr.jpl.nasa.gov/getData/accessData/. The AERONET data were obtained from

525   https://aeronet.gsfc.nasa.gov/. Data of NCEP reanalysis-2 outgoing longwave radiation

526   (OLR) were obtained from

527   https://psl.noaa.gov/data/gridded/data.ncep.reanalysis2.pressure.html. The OSIRIS aerosol

528   extinction coefficient can be downloaded from https://research-groups.usask.ca/osiris/data-

529   products.php#Download

530   **Author contributions**: S. F. initiated the idea. P. C. and T. C. performed model analysis. R

531   M., S.G and C.E.S. contributed analysis and study design. C. E. S.and S.G. analyzed OSIRIS

532   data. All authors contributed to the writing and discussions of the manuscript.

533   **Competing Interests**: The authors declare no competing interests.

References:

Abdou, W. A., Diner, D. J., Martonchik, J. V., Bruegge, C. J., Kahn, R. A., Gaitley, B. J., Crean, K. A., Remer, L. A., and B. Holben: Comparison of coincident Multiangle Imaging Spectroradiometer and Moderate Resolution Imaging Spectroradiometer aerosol optical depths over land and ocean scenes containing Aerosol Robotic Network sites, J. Geophys. Res.,110, D10S07, doi:10.1029/2004JD004693, 2005.

Andreae, M. O.: Emission of trace gases and aerosols from biomass burning – an updated assessment, Atmos. Chem. Phys., 19, 8523–8546, https://doi.org/10.5194/acp-19-8523-2019, 2019.

Banerjee A., Chiodo, G., Previdi, M., Ponater, M., Conley, A. J., Polvani L. M.: Stratospheric water vapor: an important climate feedback, Clim. Dyn., 53, 1697–1710, https://doi.org/10.1007/s00382-019-04721-4, 2019.

Bhardwaj, P. M., Naja, R., Kumar, and Chandola, H. C.: Seasonal, interannual, and long-term variabilities in biomass burning activity over South Asia, Environ. Sci. Pollut. Res, 23(5), 4397–4410, 2016.

Bond, T. C., Doherty, S. J., Fahey, D. W., Forster, P. M., Berntsen, T., Deangelo, B. J., Flanner, M. G., Ghan, S., Kärcher, B., Koch, D., Kinne, S., Kondo, Y., Quinn, P. K., Sarofim, M. C., Schultz, M. G., Schulz, M., Venkataraman, C., Zhang, H., Zhang, S., Bellouin, N., Guttikunda, S., K., Hopke P. K., Jacobson, M. Z., Kaiser, J., W., Klimont, Z., Lohmann, U., Schwarz, J. P., Shindell, D., Storelvmo, T., Warren, S. G., and Zender. C. S.: Bounding the role of black carbon in the climate system: A scientific assessment, J. Geophys. Res. Atmos.118(11):5380–5552, 2013.

Bourassa, A. E., Rieger, L. A., Lloyd, N. D., and Degenstein, D. A.: Odin-OSIRIS stratospheric aerosol data product and SAGE III intercomparison, Atmos. Chem. Phys., 12, 605–614, https://doi.org/10.5194/acp-12-605-2012, 2012.

559 Brunamonti, S., Jorge, T., Oelsner, P., Hanumanthu, S., Singh, B. B., Ravi Kumar, K.,

560   Sonbawne, S., Meier, S., Singh, D., Wienhold, F.G. , Luo, B.-P., Boettcher, M.,

561   Poltera, Y., Jauhiainen, H., Kayastha, R., Karmacharya, J., Dirksen, R., Naja, M.,

562   Rex, M., Fadnavis, S., and Peter, T.: Balloon-borne measurements of temperature,

563   water vapor, ozone and aerosol backscatter on the southern slopes of the Himalayas

564   during StratoClim 2016–2017, Atmos. Chem. Phys., 18, 15937–15957, 2018,

565   https://doi.org/10.5194/acp-18-15937-2018, 2018.

566 Chang, C-P., Wang, Z., McBride, J., and Liu, C-H : Annual Cycle of Southeast Asia—

567   Maritime Continent Rainfall and the Asymmetric Monsoon Transition, J. Clim., 287–

568   301, 18, 2005, https://doi.org/10.1175/JCLI-3257.1, 2005.

569 Chen, J. C., Li, Z., Ristovski, A., Milic, Y., Gu, M., S., Islam, S., Wang, J., Hao, H., Zhang,

570   C., He, H., Guo, H., Fu, B., Miljevic, L., Morawska, P., Thai, Y., Fat LAM, G., Pereira,

571   A., Ding, X., Huang, and Dumka. U. C.: A review of biomass burning: Emissions and

572   impacts on air quality, health and climate in China, Sci. Total Environ., 579,1000–1034,

573   2017.

574 Cheng, F. Y., Yang, Z. M., Chang, Y., and Ngan, F.: A numerical study of the dependence of

575   long-range transport of CO to a mountain station in Taiwan on synoptic weather patterns

576   during the Southeast Asia biomass-burning season, Atmos. Environ., 78, 277–90, 2013.

577 Cheng, Y. F., Berghof, M., Garland, R. M., Wiedensohler, A., Wehner, B., Müller, T., Su, H.,

578   Zhang, Y. H., Achtert, P., Nowak, A., Poschl, U., Zhu, T., Hu, M., and Zeng. L. M.:

579   Influence of soot mixing state on aerosol light absorption and single scattering albedo

580   during air mass aging at a polluted regional site in northeastern China, J. Geophys. Res.

581   Atmos., 114(11), 1–20, 2009.

582 Choi, M., Lim, H., Kim, J., Lee, S., Thomas T. E., Holben, B. B., Garay, M. J., Hyer, E. E.,

583   Saide, P. P., and Liu, H.: Validation, Comparison, and Integration of GOCI, AHI,

MODIS, MISR, and VIIRS Aerosol Optical Depth over East Asia during the 2016 KORUS-AQ Campaign, Atmos. Meas. Tech. 12 (8): 4619–41. https://doi.org/10.5194/amt-12-4619-2019, 2019.

Clough, S. A., and Iacono, M. J.: Line-by-line calculation of atmospheric fluxes and cooling rates 2. Application to carbon dioxide, ozone, methane, nitrous oxide and the halocarbons, J. Geophy. Res., 100(D8), 16,519-16,535, 1995.

Dentener, F. S., Kinne, T., Bond, O., Boucher, J., Cofala, S., Generoso, P., Ginoux, S., Gong, J., J., Hoelzemann, A., Ito, L., Marelli, J., E., Penner, J., P., Putaud, C., Textor, M., Schulz, G., R., Van Der Werf, and J., Wilson.: Emissions of primary aerosol and precursor gases in the years 2000 and 1750 prescribed data-sets for AeroCom, Atmos. Chem. and Phys., 6(12), 4321–44, 2006.

Dessler, A. E., Schoeberl, M. R., Wang, T., Davis, S. M.,and Rosenlof, K. H. Stratospheric Water Vapor Feedback, Proc. Nat. Acad. Sc. U. S. 110 (45): 18087–91. https://doi.org/10.1073/pnas.1310344110, 2013.

Dong, X., and Fu, J. S.: Understanding interannual variations of biomass burning from peninsular Southeast Asia, Part II: Variability and different influences in lower and higher atmosphere levels, Atmos. Environ., 115, 9–18, 2015.

Fadnavis, S., Chakraborty, T., Ghude S. D., Beig, G., and Raj. P. E.: Modulation of Cyclone Tracks in the Bay of Bengal by QBO, J. Atmos Terr. Phys. 73(13):1868–75, 2011.

Fadnavis, S., Semeniuk, K., Pozzoli, L., Schultz, M. G., Ghude, S. D., Das, S., and Kakatkar. R.: Transport of Aerosols into the UTLS and Their Impact on the Asian Monsoon Region as Seen in a Global Model Simulation, Atmos. Chem. and Phys. 13(17):8771–86. 2013.

Fadnavis, S., Kalita, G., Kumar, K. R., Gasparini, B., and Li, J -L. F.,: Potential Impact of Carbonaceous Aerosol on the Upper Troposphere and Lower Stratosphere (UTLS) and

609   Precipitation during Asian Summer Monsoon in a Global Model Simulation, Atmos.

610   Chem. and Phys. 17(18):11637–54, 2017a.

611 Fadnavis S., Roy, C., Sabin, T. P., Ayantika, D. C., Karumuri, A.: Potential modulations of

612   pre-monsoon aerosols during El Niño: impact on Indian summer monsoon, Clim. Dyn.,

613   49(7-8), 2017.

614 Fadnavis, S., Müller, R., Kalita, G., Rowlinson, M., Rap, A., Li, J.-L. F., Gasparini, B., and

615   Laakso, A.: The impact of recent changes in Asian anthropogenic emissions of SO_2 on

616   sulfate loading in the upper troposphere and lower stratosphere and the associated

617   radiative changes, Atmos. Chem. Phys., 19, 9989–10008, https://doi.org/10.5194/acp-

618   19-9989-2019, 2019.

619 Fadnavis, S., Sabin, T. P., Rap, A.. Müller, R., Kubin, A., and Heinold, B.: The impact of

620   COVID-19 lockdown measures on the Indian summer monsoon, Environ. Res.

621   Lett. 16, 074054, https://doi.org/10.1088/1748-9326/ac109c, 2021a.

622 Fadnavis, S., Sioris, C. E., Wagh, N., Chattopadhyay, R., Tao, M., Chavan, P., Chakroborty,

623   T.: A rising trend of double tropopause s over South Asia in a warming environment:

624   Implications for moistening of the lower stratosphere, Int. J. Climatol., 41, E200–E215,

625   DOI: 10.1002/joc.6677, 2021b.

626 Fisher, J., Jacob, A. D. J., Wang, Q., Bahreini, R., Carouge, C. C., Cubison, M. J. Dibb, J. E.

627   Diehl, T., Jimenez, J. L., Leibensperger, E. M., Lu, Z., Marcel, B., Havala, J. M., Pye,

628   O. T., Quinn, P. K., Sharma, S., Streets, D. G., Donkelaar, A., and Yantosca R. M.:

629   Sources, Distribution, and Acidity of Sulfate-Ammonium Aerosol in the Arctic in

630   Winter-Spring, Atmos. Environ., 45(39):7301–18, 2011.

631 Gettelman, A. P., Piers, M., Fujiwara, M., Fu, Q., Vömel, H., Gohar, L. K., Johanson, C., and

632   Ammerman. M.: Radiation Balance of the Tropical Tropopause Layer, J. Geophys.Res.:

633   Atmos. 109(7):1–12, 2004.

634   Giglio, L., Descloitres, J. Justice, C. O. and Kaufman, Y. J.: An Enhanced Contextual Fire

635   Detection Algorithm for MODIS, Remote Sens. of Environ. 87(2–3):273–282, 2003.

636   Giglio, L.: MODIS Collection 6 Active Fire Product User's Guide Revision A. Unpublished

637   Manuscript, Department of Geographical Sciences, University of Maryland.(

638   http://modisfire.umd.edu/files/MODIS_C6_Fire_User_Guide_A.pdf) March, 2015.

639   Guenther, A.: A Global Model of Natural Volatile Organic Compound Emissions, J. Geophys.

640   Res. 100(D5):8873–92, 1995.

641   Guha, A., Kumar, B., Dhar, D. P., Banik, T., Chakraborty, M., Roy, R., Choudhury, A.,

642   Mukunda, M., Gogoi, S., Babu, S., and Krishna Moorthy, K.: Seasonal Characteristics of

643   Aerosol Black Carbon in Relation to Long Range Transport over Tripura in Northeast

644   India, Aerosol Air Qual. Res. 15(3):786–98, 2015.

645   Guhathakurta, P., and Rajeevan, M.: Trends in the Rainfall Pattern over India, Int. J.

646   Climatol. 28(11):1453–69, 2008.

647   Hooghiem, J., Maria J. D., Popa, E., Thomas., R, Grooß, J-U. Tritscher, I., Müller, R., Kivi,

648   R., and Chen, H.: Wildfire Smoke in the Lower Stratosphere Identified by in Situ CO

649   Observations, Atmos. Chem. and Phys., 20 (22): 13985–3. https://doi.org/10.5194/acp-

650   20-13985-2020, 2020.

651   Hanumanthu, S., Vogel, B., Müller, R., Brunamonti, S., Fadnavis, S., Li, D., Ölsner, P., Naja,

652   M., Singh, B. B., Ravi Kumar, K., Sonbawne, S., Jauhiainen, H., Vömel, H., Luo, B.,

653   Jorge, T., Wienhold, F. G., Dirkson, R., and Peter, T.: Strong day-to-day variability of the

654   Asian Tropopause Aerosol Layer (ATAL) in August 2016 at the Himalayan foothills,

655   Atmos. Chem. Phys., 20, 14273–14302, 2020, https://doi.org/10.5194/acp-20-14273-

656   2020.

657   Khaykin, S. B., Legras, S., Bucci, P., Sellitto, L., Isaksen, F., Tencé, S., Bekki, A., Rieger, B.

658   L., Zawada, D., Jumelet, J., and Godin-Beekmann, S.: The 2019/20 Australian Wildfires

Generated a Persistent Smoke-Charged Vortex Rising up to 35 Km Altitude, Commu. Earth Environ., 1, 22. https://doi.org/10.1038/s43247-020-00022-5, 2020.

Lamarque, J. T., Bond, V., Eyring, C., Granier, A., Heil, Z., Klimont, D., Lee, C., Liousse, A., Mieville, B., Owen, M., G., Schultz, D., Shindell, S., J., Smith, E., Stehfest, J.,Van Aardenne, O.,R., Cooper, M., Kainuma, Mahowald, N., McConnell, J. R.,Naik, V., Riahi, K., and Vuuren, D.: Historical (1850-2000) Gridded Anthropogenic and Biomass Burning Emissions of Reactive Gases and Aerosols: Methodology and Application, Atmos .Chem. Phys., 10(15):7017–39, 2010.

Lau, W., Kim, M-k., & Kim, K.: Asian summer monsoon anomalies induced by aerosol direct forcing: The role of the Tibetan Plateau, Clim. Dyn., 26. 855-864. 10.1007/s00382-006-0114-z, 2006.

Lestrelin, H., Legras, B., Podglajen, A., and Salihoglu, M.: Smoke-charged vortices in the stratosphere generated by wildfires and their behaviour in both hemispheres: comparing Australia 2020 to Canada 2017, Atmos. Chem. Phys., 21, 7113–7134, https://doi.org/10.5194/acp-21-7113-2021, 2021.

Lin, C., Zhao, Y. C., Liu, X., Lin, N. H., and Chen, W. N.: Modelling of Long-Range Transport of Southeast Asia Biomass-Burning Aerosols to Taiwan and Their Radiative Forcings over East Asia. Tellus, Series B: Chem. Phys. Meteorol., 66(1), 23733, 2014.

Li, Z., Yang, S., He, B., and Hu, C.: Intensified Springtime Deep Convection over the South China Sea and the Philippine Sea Dries Southern China, Sci. Rep., 6, 30470, 2016.

Matson, M., and J., Dozier.: Identification of Subresolution High Temperature Sources Using a Thermal IR Sensor. Photogramm, Eng. Remote Sensing, 47(9), 1311–18, 1981.

Maycock A. C., Joshi, M. M., Shine, K. P., Scaife, A. A.: The Circulation Response to Idealized Changes in Stratospheric Water Vapor, J. Clim., 26, 545-561, DOI: 10.1175/JCLI-D-12-00155.1, 2013.

Meehl, G. A., Arblaster, J., and Collins, W. D.: Effects of Black Carbon Aerosols on the Indian Monsoon, J. Clim., 21(12),2869–82, 2008.

Mhawish, A. T., Banerjee, M., Sorek-Hamer, A., Lyapustin, D., Broday, and Chatfield, R.: Comparison and Evaluation of MODIS Multi-Angle Implementation of Atmospheric Correction (MAIAC) Aerosol Product over South Asia, Remote Sens. of Environ., 224, 12–28, 2019.

Mieville, A., Granier, C., Liousse, C., Guillaume, B., Mouillot, F., Lamarque, J. F., Grégoire, J. M., and Pétron, G.: Emissions of Gases and Particles from Biomass Burning during the 20th Century Using Satellite Data and an Historical Reconstruction, Atmos. Environ., 44(11), 1469–77, 2010.

Murugavel, P., Pawar, S. D., and Gopalakrishnan, V. : Trends of Convective Available Potential Energy over the Indian Region and Its Effect on Rainfall, Int. J. Climatol., 32(9), 1362–72, 2012.

Nguyen, H. N., Bengt, G., Martinsson, J. B., Wagner, E., Carlemalm, M., Ebert, S., Weinbruch, C., Brenninkmeijer, A. M., Heintzenberg, J., Hermann, M., Schuck, T., van Velthoven, P. F. J., and Zahn, A.: Chemical Composition and Morphology of Individual Aerosol Particles from a CARIBIC Flight at 10 Km Altitude between 50°N and 30°S, J. Geophy. Res. Atmos., 113(23), 1–12, 2008.

Ni, H., Huang, R-J, Cao, J., Guo, J., Deng, H, and Dusek, U.: Sources and formation of carbonaceous aerosols in Xi'an, China: primary emissions and secondary formation constrained by radiocarbon, Atmos. Chem. Phys., 19, 15609–15628, https://doi.org/10.5194/acp-19-15609-2019, 2019.

Oman, L., D., Waugh, S., Pawson, R. S., Stolarski, and Nielsen, J. E.: Understanding the Changes of Stratospheric Water Vapor in Coupled Chemistry-Climate Model Simulations, J. Atmos. Sci., 65(10), 3278–91, 2008.

709 Oshima, N., Kondo, Y., Moteki, N., Takegawa, N., Koike, M., Kita, K., Matsui, H., Kajino,

710   M., Nakamura, H., Jung, J. S., and Kim, Y. J.: Wet Removal of Black Carbon in Asian

711   Outflow: Aerosol Radiative Forcing in East Asia (A-FORCE) Aircraft Campaign, J.

712   Geophy. Res. Atmos., 117(3), 1–24, 2012.

713 Peterson, D. A., Campbell J. R., Edward, J. H., Michael, D. F., George, P. K., Cossuth, J. H.,

714   and Matthew, T. D.: Wildfire-Driven Thunderstorms Cause a Volcano-like Stratospheric

715   Injection of Smoke, Npj Clim. Atmos. Sci., 1(1), 1–8, 2018.

721 Pozzoli, L., Bey I., Rast, S., Schultz, M. G. Stier, P., and Feichter, J.: Trace gas and aerosol

722   interactions in the fully coupled model of aerosol-chemistry-climate ECHAM5-

723   HAMMOZ: 1. Model description and insights from the spring 2001 TRACE-

724   Pexperiment, J. Geophys. Res., 113, D07308, doi:10.1029/2007JD009007, 2018.

725 Randel, W. J., Park, M., Emmons, L., Kinnison, D., Bernath, P., Walker, K. A., Boone, C.,

726   and Pumphrey H.: Asian Monsoon Transport of Pollution to the Stratosphere, Sci.,

727   328(5978), 611–13, 2010.

728 Rieger, L, A., Malinina, E. P., Rozanov V., Burrows J. P., Bourassa A. E., and Degenstein D.

729   A.: A study of the approaches used to retrieve aerosol extinction, as applied to limb

730   observations made by OSIRIS and SCIAMACHY, Atmos. Meas. Tech., 11, 3433–3445,

731   https://doi.org/10.5194/amt-11-3433-2018, 2018.

732 Riese, M., Ploeger, F., Rap, A., Vogel, B., Konopka, P., Dameris, M., and Forster, P.: Impact

733   of uncertainties in atmospheric mixing on simulated UTLS composition and related

734   radiative effects, J. Geophys. Res., 117, D16305, doi:10.1029/2012JD017751, 2012.

735 Schill, G. P., Froyd, K. D., Bian, H., Kupc, A., Williamson, C., Brock, C. A., Ray, E.,

736   Hornbrook, R. S., Hills, A. J., Apel, E. C., Chin, M., Colarco, P. R., and Murphy, D. M.:

737   Widespread Biomass Burning Smoke throughout the Remote Troposphere, Nat. Geosci.,

738   13(6), 422–27, 2020.

Schultz, M. G., Heil, A., Hoelzemann, J. J., Spessa, A., Thonicke, K., Goldammer, J. G., Alexander, C. H., Pereira, J. M. C., and Bolscher, M.: Global Wildland Fire Emissions from 1960 to 2000, Global Biogeochem. Cycles, 22(2), 1–17, 2008.

Sherwood, S., Dixit, V., and Salomez, C.: The Global Warming Potential of Near-Surface Emitted Water Vapour, Environ. Res. Lett., 13(10), 104006, 2018.

Shindell, D., Chin, T. M., Dentener, F., Doherty, R. M., Faluvegi, G., Fiore, A. M., Hess, P., Koch, D. M., MacKenzie, I. A., Sanderson, M. G., Schultz, M. G., Schulz, M., Stevenson, D. S., Teich, H., Textor, C., Wild, O., Bergmann, D., J., Bey, I., Bian, H., Cuvelier, C., Duncan, B. N., Folberth, G., Horowitz, L. W., Jonson, J., Kaminski, J. W., Marmer, E., Park R.,, Pringle, K. J., Schroeder, S., Szopa, S., Takemura, T., Zeng, G., Keating, T. J.,and Zuber. A.: A Multi-Model Assessment of Pollution Transport to the Arctic, Atmos. Chem. Phys., 8(17), 5353–72, 2008.

Singh, N., Murari, V., Kumar, M., Barman, S. C., and Banerjee, T.: Fine Particulates over South Asia: Review and Meta-Analysis of PM2.5 Source Apportionment through Receptor Model, Environ. Pollut., 223, 121–136, 2017.

Singh, P., Sarawade, P., and Adhikary, B.: Transport of Black Carbon from Planetary Boundary Layer to Free Troposphere during the Summer Monsoon over South Asia. Atmos. Res., 235, 104761, 2020.

Singh, P., Sarawade, P., and Adhikary, B.: Carbonaceous Aerosol from Open Burning and Its Impact on Regional Weather in South Asia, Aerosol Air Qual. Res., 20(3), 419–31, 2020.

Stier, P., Feichter, J., Kinne, S., Kloster, S., Vignati, E., Wilson, J., Ganzeveld, L.: The Aerosol-Climate Model ECHAM5-HAM, Atmos. Chem. Phys., 5(4), 1125–1156, https://doi.org/10.5194/acp-5-1125-2005, 2005.

Streets, D. G., Yarber, K. F., Woo, J. H., and Carmichael, G. R.: Biomass Burning in Asia: Annual and Seasonal Estimates and Atmospheric Emissions, Global Biogeochem.

Cycles, 17(4), 1099, doi:10.1029/2003GB002040, 2003.

Talukdar, S., Jana, S., Maitra, A., and Gogoi, M. M. : Characteristics of Black Carbon Concentration at a Metropolitan City Located near Land-Ocean Boundary in Eastern India, Atmos. Res., 153, 526–34, 2015.

Tegen, I., Neubauer, D., Ferrachat, S., Drian, C., Bey, I., Schutgens, N., Stier, P., Duncan, W. P., Stanelle, T., Schmidt, H., Rast, S., Kokkola, H., Schultz, M., Sabine, S., Daskalakis, N., Barthel, S., Heinold, B., and Lohmann, U.: The Global Aerosol-Climate Model Echam6.3-Ham2.3 -Part 1: Aerosol Evaluation, Geosci. Model Dev., 12(4), 1643–77, 2019.

Textor, C., Schulz, M., Guibert, S., Kinne, S., Balkanski, Y., Bauer, S., Berntsen, T., Berglen, T., Boucher, O., Chin, M., Dentener, F., Diehl, T., Easter, R., Feichter, H., Fillmore, D., Ghan, S., Ginoux, P., Gong, S., Grini, A., Hendricks, J., Horowitz, L., Huang P. Isaksen I., Iversen, I., Kloster, S., Koch, D., Kirkevåg, A., Kristjansson, J. E., Krol, M., Lauer, A. Lamarque, J. F., Liu, X., Montanaro, V., Myhre, G., Penner, J., Pitari, G., Reddy, S., Seland, Ø., Stier, P., Takemura, T., and Tie, X.: Analysis and quantification of the diversities of aerosol life cycles within AeroCom, Atmos. Chem. Phys., 6, 1777–1813, 2006, https://doi.org/10.5194/acp-6-1777-2006.

Thomas, A., Sarangi, C., and Kanawade, V. P.: Recent Increase in Winter Hazy Days over Central India and the Arabian Sea, Sci. Rep., 9(1), 1–10, 2019.

Val Martin, M., Logan, J. A., Kahn, R. A., Leung, F.-Y., Nelson, D. L., and Diner, D. J.: Smoke injection heights from fires in North America: analysis of 5 years of satellite observations, Atmos. Chem. Phys., 10, 1491–1510, https://doi.org/10.5194/acp-10-1491-2010, 2010.

Van Der Werf, G. R., Randerson, J. T., Giglio, L., Collatz, G. J., Kasibhatla, P. S.,and Arellano, A. F.: Interannual Variability in Global Biomass Burning Emissions from 1997

to 2004, Atmos. Chem. and Phys., 6(11), 3423–41, 2006.

Wang, S. H., Lin, N. H., Chou, M. D., and Woo. J. H.: Estimate of Radiative Forcing of Asian Biomass-Burning Aerosols during the Period of TRACE-P, J. Geophys. Res. Atmos., 112(10), 1–17, 2007.

Wang, S. H., Ellsworth, J. W., Holben, B. N., Tsay S. C.,, Lin, N. H., Giles, D., Sebastian, A. S., Xuan, S. J., Nguyen, A., Hsiao, T., Chen, W. N., Lin, T. H,. Buntoung, S. S. C., and Wiriya. W.: Vertical Distribution and Columnar Optical Properties of Springtime Biomass- Burning Aerosols over Northern Indochina during 2014 7-SEAS Campaign, Aerosol Air Qual. Res., 15(5), 2037–50, 2015.

Weigel, R., Mahnke, C., Baumgartner, M., Dragoneas, A., Vogel, B., Ploeger, F., Viciani, S., D'Amato, F., Bucci, S., Legras, B., Luo, B., and Borrmann, S.: In situ observation of new particle formation (NPF) in the upper troposphere/lower stratosphere of the 2017 Asian monsoon anticyclone, Part 1: Summary of StratoClim results, Atmos. Chem. Phys. , https://doi.org/10.5194/acp-21-11689-2021, 2021.

Wu, J., Kong, S., Wu, F., Cheng, Y., Zheng, S., Yan, Q., Zheng, H., Yang, G., Zheng, M., Liu, D., Zhao, D., and Qi, S.: Estimating the Open Biomass Burning Emissions in Central and Eastern China from 2003 to 2015 Based on Satellite Observation, Atmos. Chem. Phys., 18(16), 11623–46, 2018.

Xie, F., Tian, W., Zhou, X., Zhang, J., Xia, Y., and Lu, J.: Increase in Lower Stratospheric Water Vapor in the Past 100 Years Related to Tropical Atlantic Warming, Geophys. Res. Lett., 47, e2020GL090539. https://doi.org/10.1029/2020GL090539, 2020.

Zhang, X., Liu, J., Han, H., Zhang, Y., Jiang, Z., Wang, H., Meng, L., Li, Y. C., and Liu Y.: Satellite-Observed Variations and Trends in Carbon Monoxide over Asia and Their Sensitivities to Biomass Burning, Remote Sens. 12(5), 2020.
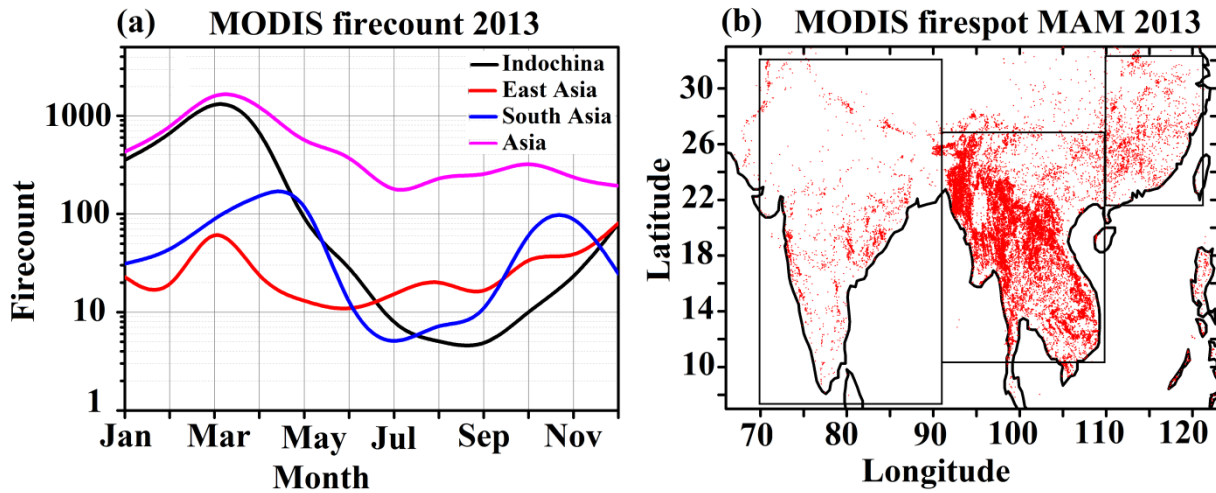
Figure 1: (a) Monthly mean distribution of MODIS fire counts averaged over Indochina (91ºE - 107ºE, 10ºN - 27ºN), East Asia (108ºE - 123ºE, 22ºN - 32ºN), South Asia (70ºE - 90ºE, 8^{0}N - 32^{0}N) and Asia (60ºE - 130ºE, 10ºS - 50ºN) (b) Spatial distribution of fire spots over South Asia, Indochina and East Asia averaged for spring 2013. Boxes in Figure (b) indicate the boundaries of South Asia, Indochina, and East Asia.
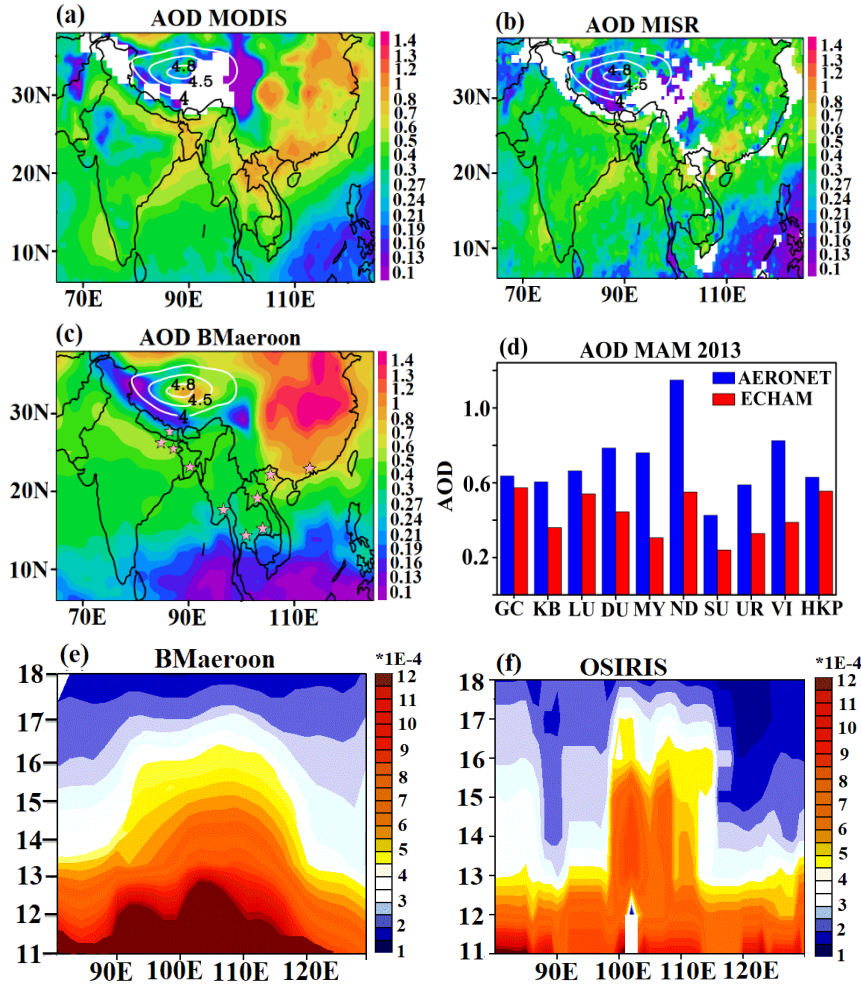
Figure 2: (a) Aerosol optical depth (AOD) averaged for spring 2013 from MODIS, (b) same as (a) but from MISR, (c) same as (a) but from ECHAM6 - HAMMOZ BMaeroon simulation. White contours in Fig (a)-(c) indicate the orography (km) of the Tibetan Plateau, (d) Comparison of simulated AOD (from BMaeroon) averaged for spring 2013 with AERONET observations at Gandhi college (GC; 25.81°N - 85.12°E), Kathmandu Bode (BD; 27.68°N - 85.39°E), Lumbini (LU; 27.49°N - 83.28°E), Dhaka University (DU; 23.72°N - 90.39°E), Myanmar(MY; 16.86°N-96.15°E), Nghia Do (ND; 21.04°N - 105.80°E), Silpakorn University (SU; 13.81°N - 100.04°E), Ubon Ratchathani (UR; 15.24°N - 104.87°E), Vientiane (VI; 17.99°N - 102.57°E), Hong Kong Poly (HKP; 22.30°N – 114.18°E). (e) Simulated (BMaeroon) aerosol extinction coefficient (865 nm) (km^{-1}), averaged for 12°N - 30°N and spring 2013 (f) same as (e) but from OSIRIS measurements (750 nm).

850

8
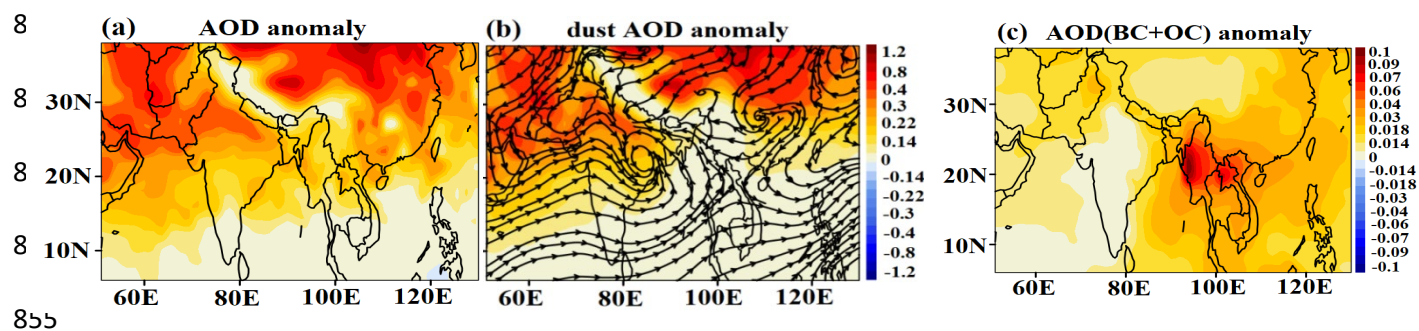
Figure 3: Distribution of ECHAM6-HAMMOZ simulated anomalies of (BMaeroon - BMaerooff) (a) AOD, (b) dust AOD, (c) BC-AOD and OC-AOD, together, averaged for spring 2013. Streamlines in figure 3b indicate wind anomalies at 900 hPa (BMaeroon-BMaerooff).
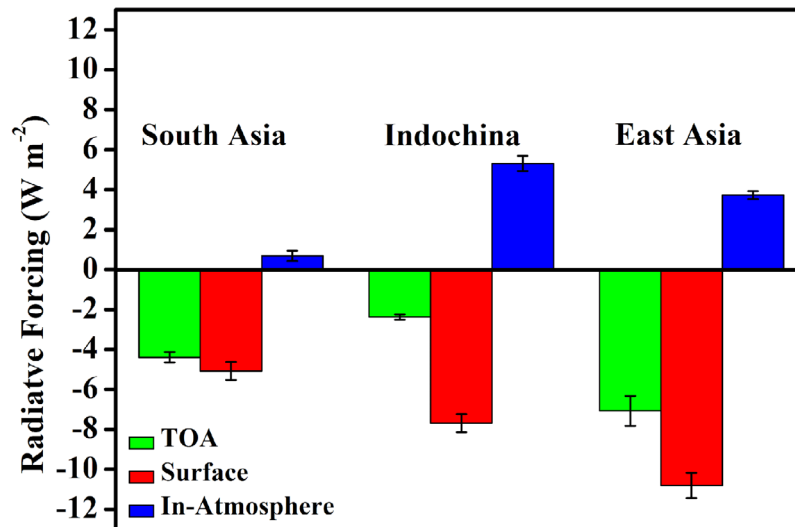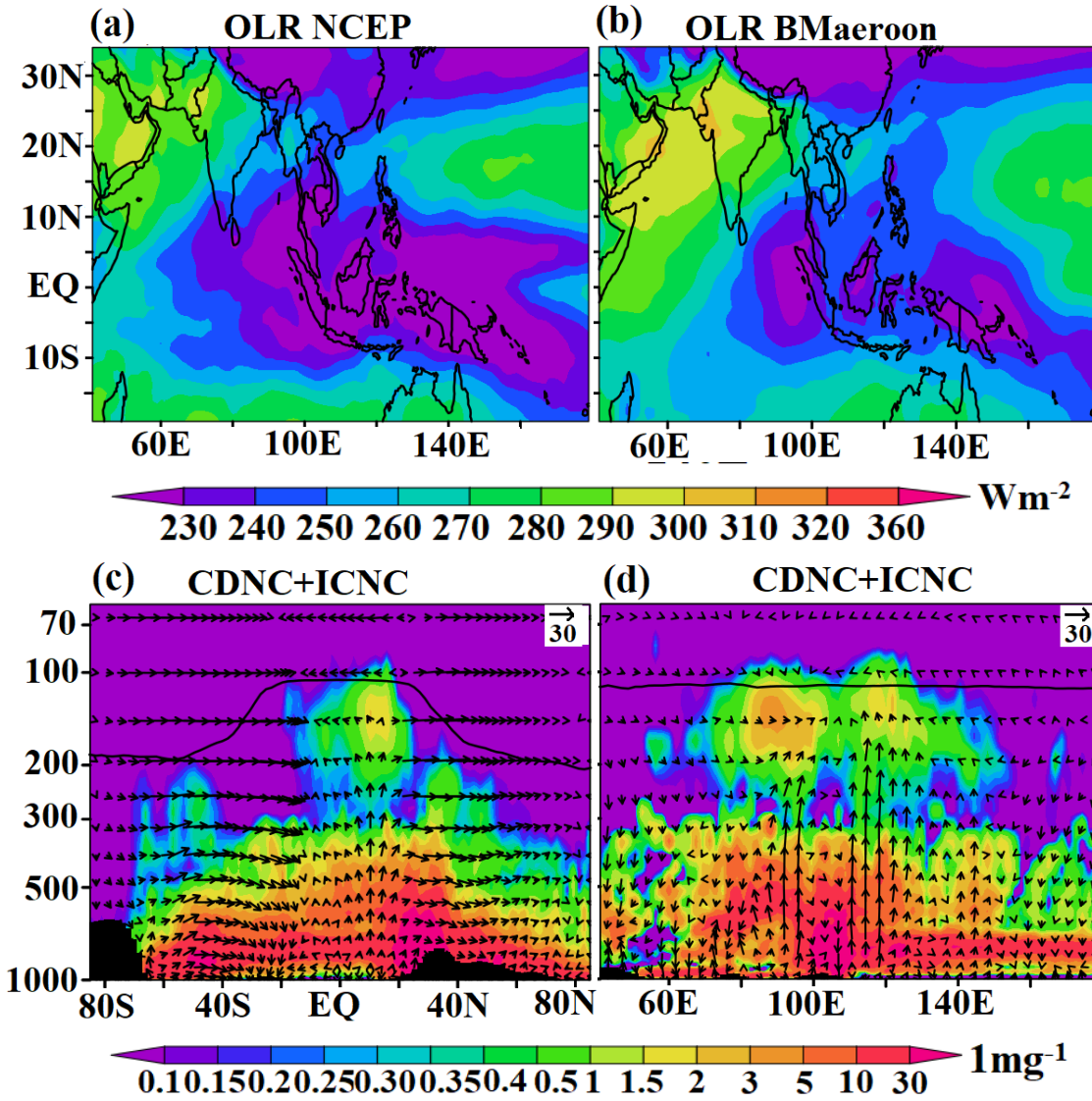
Figure 4: Anomalies of radiative forcing (W.m^{-2}) from ECHAM6-HAMMOZ simulations (BMaeroon - BMaerooff) at the TOA, surface, and in-atmosphere (TOA - Surface) averaged for spring 2013 and over South Asia, Indochina, and East Asia.

Figure 5: (a) Distribution of Outgoing Longwave Radiation (OLR) (W m^{-2}) from NCEP reanalysis-2 data averaged for spring 2013, (b) same as (a) but from the ECHAM6-HAMMOZ simulations (BMaeroon). Vertical distribution of cloud droplet number concentration (CDNC) and ice crystal number concentration (ICNC) (1 mg^{-1}) averaged for spring 2013 from ECHAM6-HAMMOZ simulations (BMaeroon) (c) latitude-pressure section (average for 85^{0}E-140^{0}E) and (d) longitude-pressure section (average for 10°N - 20°N). Vectors of the circulation (BMaeroon) are shown in (c)-(d) with the vertical velocity field scaled by 300.
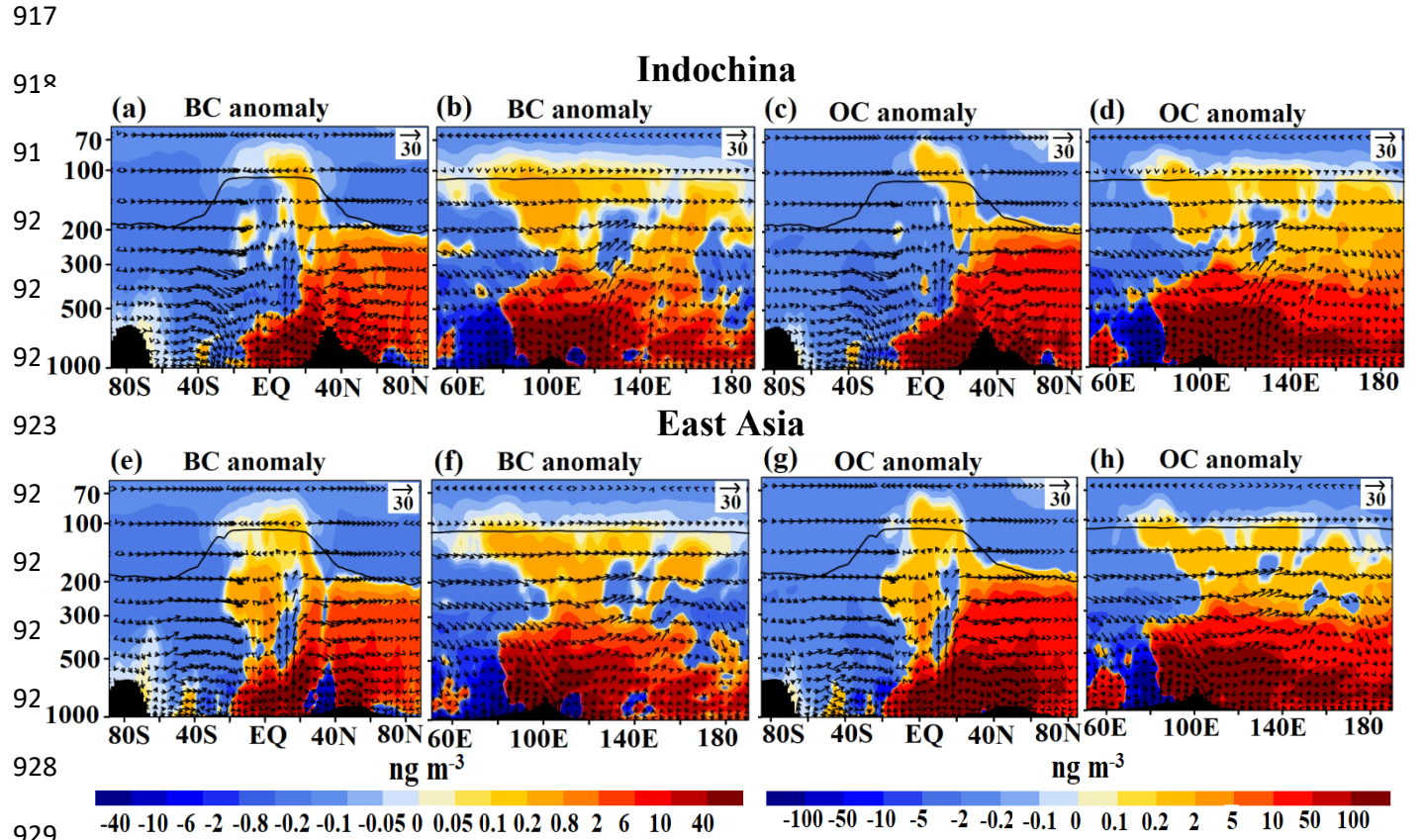
Figure 6: Vertical cross-section of anomalies of BC (ng m^{-3}) (BMaeroon – Bmaerooff) averaged for spring 2013 (a) latitude-pressure section (averaged for 91°E-107°E), (b) longitude-pressure section (averaged for 18°N-24°N). (c-d) is the same as (a-b) but for OC. (e) same as (a) but averaged over 108°E-123°E, (f) same as (b) but averaged for 18°N-24°N. (g-h) same as in (e-f) but for OC. 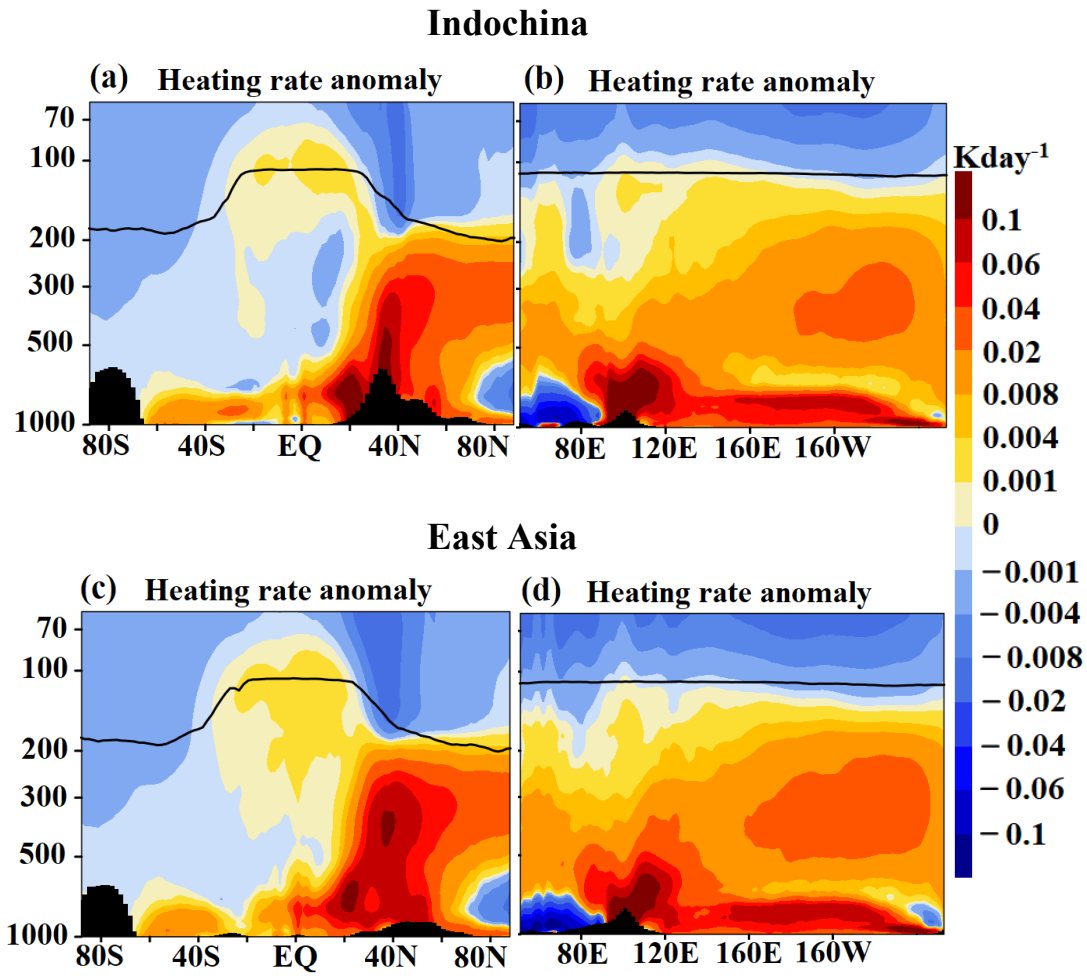The arrows in (a-h) indicate winds in m s^{-1} with the vertical velocity field scaled by 300. The black vertical bars show the topography and the black line indicates the tropopause.
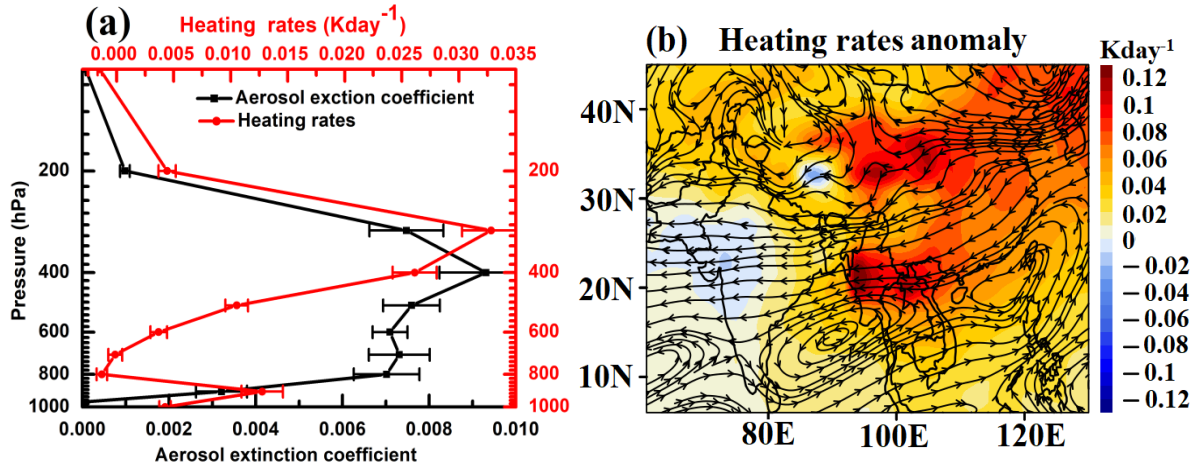
**Figure 7**: (a) Vertical profile of anomalies of extinction (km^{-1}) and heating rate (K day^{-1}) over the Arctic region (65°N-85°N) from the ECHAM6-HAMMOZ simulations (BMaeroon - BMaerooff). The horizontal lines indicate the standard deviation within the 10 members of the different initial conditions, (b) spatial distribution of anomalies of heating rates (K.day^{-1}) (short and long wave together) averaged from the surface to the tropopause. Streamlines in (b) indicate wind anomalies at 500 hPa (BMaeroon- BMaerooff).

Indochina

Figure 8: Vertical section of heating rate anomalies (K day^{-1}) for spring season 2013 from ECHAM6-HAMMOZ simulations (BMaeroon - BMaerooff) (a) latitude-pressure section averaged for $91^{o}E$-$107^{0}E$, (b) longitude-pressure section averaged for $18^{0}N$-$24^{0}N$. (c) same as (a) but averaged for $108^{o}E$-$123^{0}E$. (d) same as (b) but averaged for $22^{0}N$-$27^{0}N$. The black vertical bars show the topography and the black line indicates the tropopause.
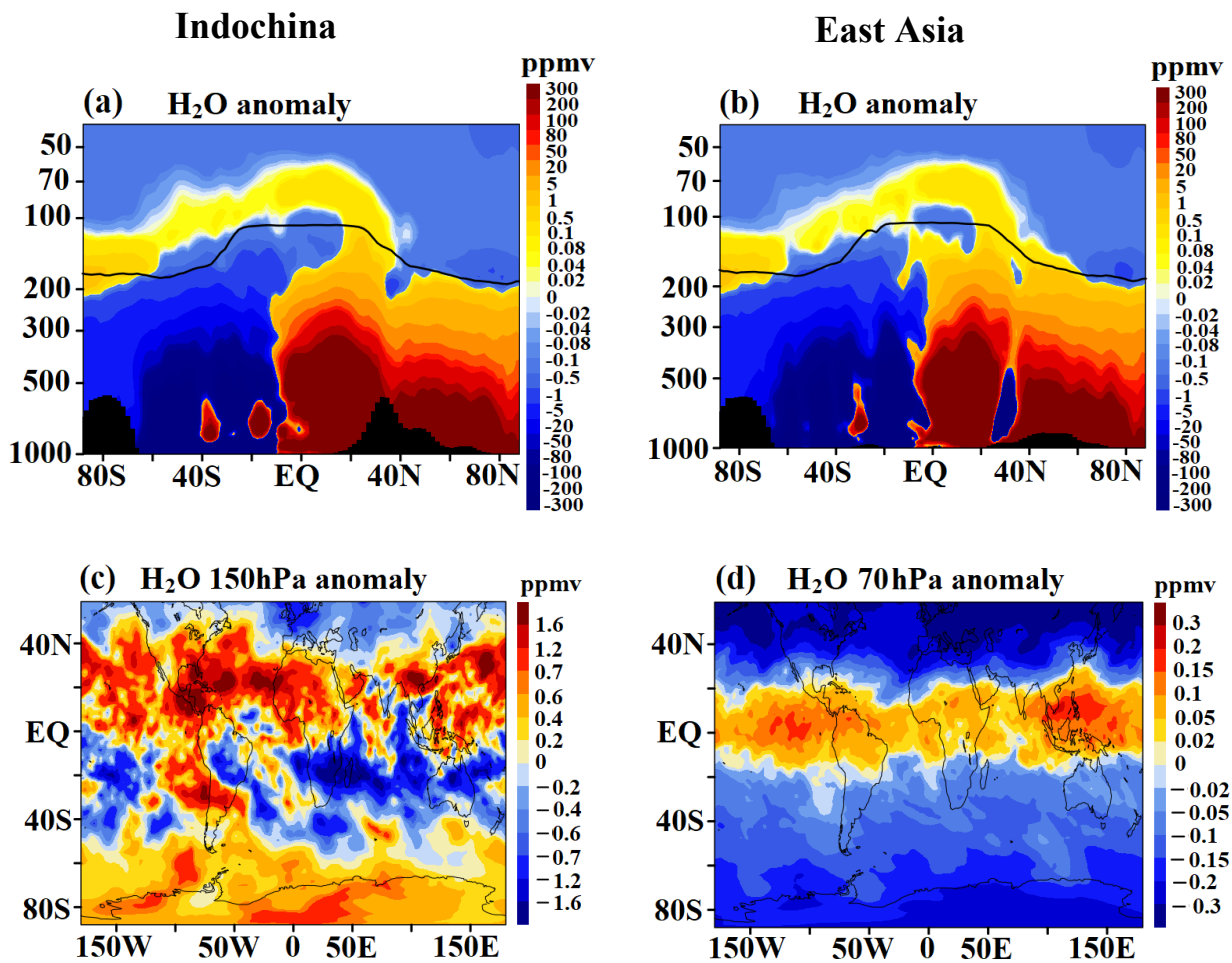
Figure 9: Vertical and horizontal distribution of anomalies of water vapour (ppmv) for spring 2013 from the ECHAM6-HAMMOZ simulations (BMaeroon - BMaerooff) (a) latitude-pressure cross-section averaged for 91°E-107°E, (b) longitude-pressure cross-section averaged over 108°E-123°E, at (c) 150 hPa level, and (d) 70 hPa level. In Fig (a)-(b) the black vertical bars show the topography and the black line indicates the tropopause.